Kinetic Modeling of Grain Boundary Cementite Evolution

M. VOGRIC, E. KOZESCHNIK, J. SVOBODA, M. FÜHRER, J. KREYCA, W. WEI, and E. POVODEN-KARADENIZ

Prediction of grain boundary cementite growth kinetics in hypereutectoid steels is necessary to control its thickness. It is a question of major industrial importance but has remained unresolved to date. This paper presents and compares two different and new modeling approaches. The first one relies on diffusion-based nucleation and growth of cementite precipitates using a modified SFFK model with short-circuit grain boundary diffusion and accounting for heterogeneous nucleation site energy during isothermal treatments and continuous cooling. It is compared to previously published simulations of diffusion-controlled reaction with moving phase boundaries and a similar simulation using the software Dictra. The second approach implies that cementite thickening is driven by the nucleation of ledges at the stepped austenite/cementite interface, controlled by a structure barrier to ledge formation previously assumed in the literature.[1] We suggest a semi-empirical formulation of this barrier to ledge nucleation during isothermal transformation. Both approaches lead to an excellent match to experimental data for an almost pure Fe–C system. This implies that modeling the stepped structure of the austenite/cementite interface is not imperative for simulation of thickening kinetics, but also that understanding the governing physics of ledge formation allows for a comprehensive description of secondary cementite formation.

I. INTRODUCTION

HYPEREUTECTOID steels are particularly interesting for industrial applications, which require a combination of good hardness and strength, for example wires or springs.[2,3] This is due to their pearlitic microstructure, constituted of alternating lamellae of ferrite and cementite formed by diffusion-controlled growth,[4] and the formation of hard proeutectoid (also called secondary) cementite due to their high carbon concentration. Depending on the grain size, reaction time, and temperature, this phase may form as grain boundary precipitates, also denoted as allotriomorphs, or as Widmanstätten precipitates. Grain boundary cementite precipitates show a dendritic appearance. They are nucleating at the grain boundary edges and corners,[5,6] impinging and forming a—continuous or fragmented—film on the austenite grain boundaries. In contrast, Widmanstätten cementite is composed of plates or laths growing from the grain boundary into the austenite grain.[7]

Understanding and controlling the characteristics of grain boundary cementite is important to improve the mechanical properties of hypereutectoid steels. Despite its hardness, cementite is brittle; thus, a thick film is deleterious to the material's toughness. Two relevant strategies exist to avoid this problem: the first is to break the continuity of the cementite film by the action of alloying elements such as Si or V[8,9] to hinder fracture propagation along the grain boundaries. The second is to reduce the thickness of the cementite film to increase its ductility, similar to the transition of pearlitic cementite from brittle to plastic with decreasing thickness.[10] The latter requires a clear understanding of the kinetics of grain boundary cementite growth, which is, however, subject of debate since the early work of Heckel and Paxton in 1960[11] and the identification of ledges at the

M. VOGRIC, M. FÜHRER, and W. WEI are with the Christian Doppler Laboratory for Interfaces and Precipitation Engineering CDL-IPE, Institute of Materials Science and Technology, TU Wien, 1060 Vienna, Austria. E. KOZESCHNIK is with the Institute of Materials Science and Technology, TU Wien, 1060 Vienna, Austria. Contact e-mail: marko.vogric@tuwien.ac.at J. SVOBODA is with the Institute of Physics of Materials, Academy of Science of the Czech Republic, 616 00 Brno, Czech Republic. J. KREYCA is with the voestalpine Forschungsservicegesellschaft Donawitz GmbH, 8700 Leoben, Austria. E. POVODEN-KARADENIZ is with the Christian Doppler Laboratory for Interfaces and Precipitation Engineering CDL-IPE, Institute of Materials Science and Technology, TU Wien and also with the Institute of Materials Science and Technology, TU Wien.

austenite/cementite boundary by Ando and Krauss in 1981.[12] The different models presented in the literature systematically overestimate the grain boundary cementite thickness at all isothermal reaction time steps for all investigated systems, including almost pure Fe–C binary alloys.[1,11] This latter point suggests that the issues in the modeling of cementite thickening kinetics are not only due to an effect of alloying elements, but to a more fundamental problem in the understanding of the phase transformation.

After reviewing the published modeling and simulation studies, the present work introduces two different approaches to modeling grain boundary cementite thickening kinetics during isothermal heat treatments, both leading to an improved matching between simulation and experimental data. The first approach is founded on classical nucleation theory and the simulation of diffusion-controlled cementite precipitation at the austenite grain boundaries following the work by Kozeschnik et al.[13–16] The second approach relies on the assumptions of partial control of the thickening kinetics by interfacial ledges and of the existence of an "interfacial structure barrier to growth" preventing the formation of new ledges at longer reaction times.[1,6] This introduces a time-dependent effective energy barrier for autocatalytic ledge production. Both approaches are evaluated for a pure Fe–C hypereutectoid steel, and their respective advantages and limitations are discussed in the following chapters.

II. REVIEW OF GRAIN BOUNDARY CEMENTITE GROWTH KINETICS

A. *The Growth Kinetics Models*

Heckel and Paxton published the first systematic experimental study on grain boundary cementite thickening kinetics during isothermal reactions.[11] Their model is based on the diffusion-controlled formation of a cementite shell on the surface of spherical austenite grains, with constant carbon diffusivity inside austenite and uniform cementite thickness. They did not consider a particular ordered morphology of the austenite/cementite phase boundary. Instead, they assumed a simple interface movement via addition of iron and carbon atoms to the cementite lattice, respectively, in a 3:1 ratio. With the balance between the loss of carbon from austenite and the carbon gain of cementite at a given time step of the reaction, they obtained the following:

$$d = R\left(1 - \left(\frac{C_{cem} - C_i}{C_{cem} - C_m}\right)^{\frac{1}{3}}\right), \quad [1]$$

where d is the grain boundary film half-thickness, R the spherical grain radius, C_{cem} the carbon concentration of cementite, C_i the initial carbon concentration in austenite, and C_m the mean carbon concentration in austenite at the considered reaction time. The reason for the use of the cementite half-thickness is that each grain in the system provides carbon for the formation

of only half of the cementite shell at a given position of the grain boundary, the neighboring grain providing carbon for the other half. The use of d instead of full thickness thus allows considering the kinetics of growth for individual grains. C_m is a function of growth time t and can be calculated according to Crank[17]:

$$\frac{C_i - C_m}{C_i - C_0} = 1 - \frac{6}{\pi^2}\sum_{n=1}^{\infty}\frac{1}{n^2}\exp\left(\frac{-Dn^2\pi^2 t}{R}\right), \quad [2]$$

where D is the diffusivity of carbon in austenite and C_0 is the equilibrium concentration of carbon in austenite. The initial time $t = 0$ is defined as the time when cementite nucleation starts. This model is compared with experimental results for isothermal treatments of Si–Mn-alloyed hypereutectoid steels at varying aging temperatures and grain sizes and at 800 °C for almost pure Fe–C steel in Figure 1.

Simulations with the Heckel–Paxton model lead to an overestimation of the cementite growth rate for all tested systems, see Figure 1. The suggested explanation for the sluggish experimental growth was the combination of high carbon flux to the interface and a slow reaction rate due to complex crystallographic rearrangements between austenite and cementite. These would lead to a decreased carbon gradient between both sides of the austenite/cementite interface compared to equilibrium and, thus, to a reduced growth rate. Alloying elements with low solubility in cementite, such as Si, would then additionally delay the growth because of the necessity for pushing them ahead of the moving interface and their effect on increasing carbon activity in austenite.

These first observations were later completed by the work of Ando and Krauss on the grain boundary cementite growth kinetics in AISI 52,100 Cr–Mn–Si containing steel grade.[12] These authors noticed that the experimental final grain boundary cementite thickness was two to four times lower than expected from equilibrium, see Figure 2a.

They also noticed that the growth kinetics followed neither the linear nor the parabolic growth law but the equation:

$$d = At^b \quad [3]$$

with A and b being constants, b varying from 0.1 to 0.25 depending on the considered alloy and reaction temperature. Equation [3] represents the logarithm of the cementite thickness as a linear function of the logarithm of time, see Figure 2b. Further, Ando and Krauss found that the measured sharp drop of carbon concentration in austenite next to the phase boundary was in disagreement with the expected flat concentration profile due to diffusion-controlled cementite growth considering the low experimental thickening rates. Ando and Krauss suggested that the sluggish cementite thickening at late reaction stages was due to the partitioning of Cr between austenite and cementite, whereas it would not occur at early growth stages. However, it was clear that this explanation could not answer the sluggish cementite
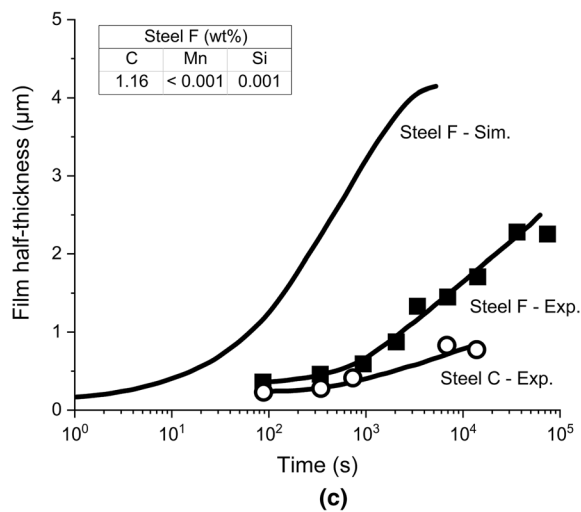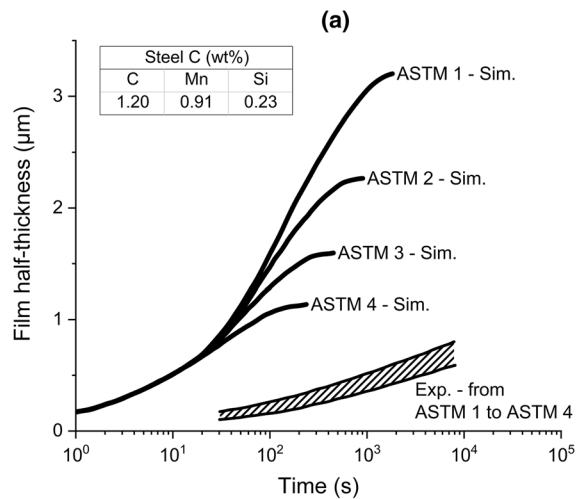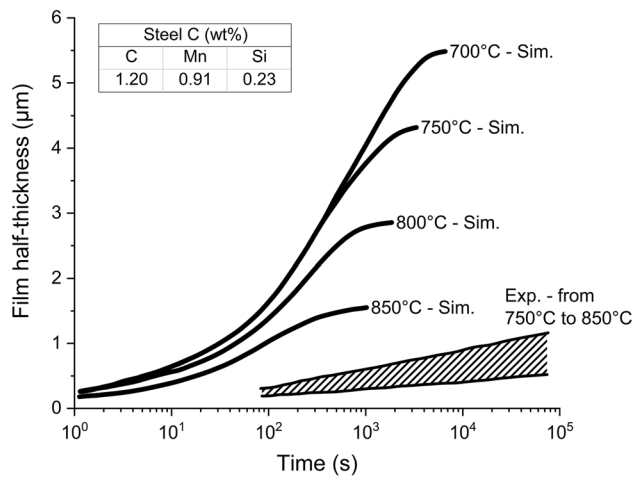
Fig. 1—Experimental (exp.) and simulated (sim.) time evolution of the grain boundary cementite half-thickness during isothermal treatment of a Fe–C–Mn–Si steel for different reaction temperatures (a), grain sizes (b), and almost pure Fe–C system (c). (Adapted from Ref. 11).
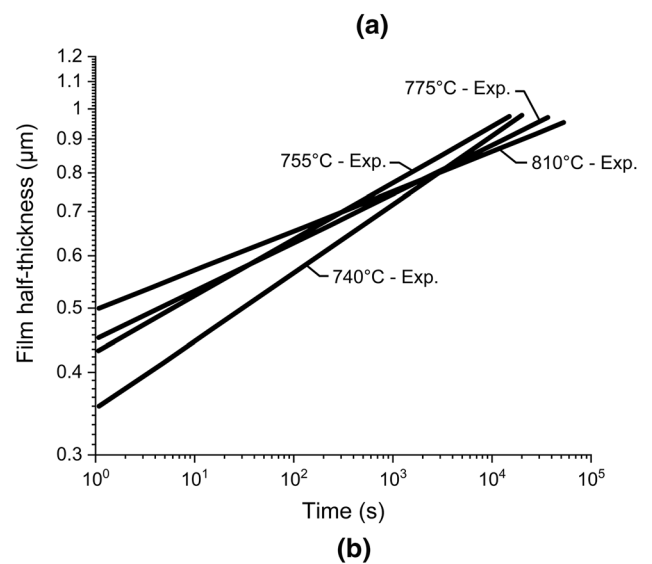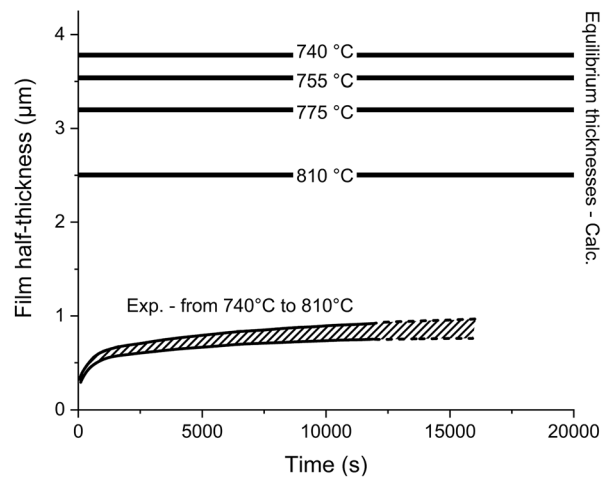

Fig. 2—Experimental (exp.) time evolution of the grain boundary cementite half-thickness during isothermal treatment of AISI 52,100 steel at different temperatures, with linear timescale and compared to calculated (calc.) equilibrium half-thicknesses (a) and with logarithmic timescale (b). (Adapted from Ref. 12).

Spanos *et al.*[1] claimed that the only remaining reason for such a slow kinetic evolution for a pure Fe–C alloy in the case of diffusion-controlled growth would be an overlapping of carbon diffusion fields of grain boundary cementite precipitates at opposite sides of the austenite grain, also called soft impingement. They verified this idea using the so-called Vandermeer model* with

*The Vandermeer model was presented as unpublished in the work of Spanos *et al.* [1] but was probably similar to the published model used by Vandermeer for the growth of proeutectoid ferrite [43], since the latter was also based on diffusion control of the movement of a disordered interface, and could take into account soft impingement.

thermodynamic Calphad input data by Gustafson[18] and the experimental data of the pure Fe–C system by Heckel and Paxton.[11] Still, the experimental growth times remained more than an order of magnitude longer than the simulated growth times, see Figure 3.

growth observed in the almost pure Fe–C system by Heckel and Paxton.[11]

Soft impingement was, thus, not a sufficient explanation for the sluggish cementite growth. Spanos *et al.* consequently concluded that diffusion control is not sufficient to describe this transformation and that there must be an "interfacial structure barrier to growth" at the austenite/cementite phase boundary,[1,6] consistent with the previous suggestion of slow reaction rate due to atomic rearrangements by Heckel and Paxton.[11]

B. *The Austenite/Cementite Interface*

In an early work, Heckel and Paxton[19] found that the morphology of the proeutectoid cementite precipitates in general coincided well with the Dubé classification for proeutectoid ferrite given minor modifications from Aaronson.[20] This means that cementite could take the form of allotriomorphs (grain boundary precipitates), primary or secondary Widmanstätten sideplates or sawteeth, idiomorphs (equiaxed crystals mostly intragranular), intragranular Widmanstätten plates or needles, or massive structures (impinged precipitates within the matrix grains). However, the actual morphology of the austenite/cementite interface played no role in developing their grain boundary cementite thickening model.[11] Nevertheless, several later studies started to use—and continue to do so to this day—the theory of ledge mechanism of growth (or ledgewise growth)[21,22] to describe the evolution of phases forming at the grain boundary, for instance, Widmanstätten or other plate precipitates,[23–25] and the growth of proeutectoid ferrite.[26,27] As first presented by Aaronson[20] and summarized by Shiflet *et al.*,[28] ledge formation is a consequence of the solid-state formation of a new phase in a crystal when coherency between the nucleus and the matrix cannot be maintained due to increasing lattice mismatch during growth. The mobility of boundary orientations with better atomic coherency diminishes, whereas boundaries with *lower* coherency experience

higher atomic attachment rates and higher mobility, resulting in a stepped morphology. Such a stepped phase boundary is denoted *ordered* as opposed to a *disordered* interface without regular morphological order between phases.

This led Ando and Krauss[12] to investigate the austenite/cementite phase boundary with grain boundary cementite present more accurately. They documented the appearance of steps at the interface along the austenite grain boundary using scanning (SEM) and transmission electron microscopy (TEM), see Figure 4. These features supported the ledgewise growth mechanism of grain boundary cementite allotriomorphs.[12] Indicative from their microstructural observations, they suggested an interface configuration comprised of large, partially coherent facets with low mobility, see Figure 5. The idea of Ando and Krauss[12] was that, since several previous studies had reported that the habit plane of Widmanstätten cementite plates was non-unique,[29] a similar situation should occur for grain boundary cementite: the different facets should correspond to different habit planes or variants. An additional type of fine incoherent facets would then exist at the surface of the large facets (as represented in Figure 5) with sufficiently large mobility to allow the cementite film to grow.[12] Spanos *et al.*[1] noted, however, that the

Fig. 4—Micrographs of grain boundary cementite from SEM showing large ledges on partially coherent steps at the phase boundary (white arrows) (*a*), and from TEM showing fine ledges (indicated by black arrows) and an impingement boundary (white arrow) (*b*). (Reprinted with permission from Ref. 12.).
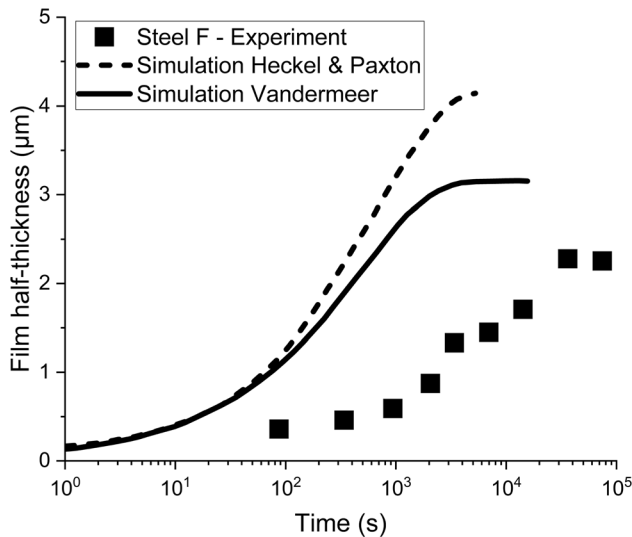
Fig. 3—Comparison between the simulated grain boundary cementite half-thickness using the Vandermeer model[1] and the experimental and simulated half-thickness obtained by Heckel and Paxton for a pure Fe–C alloy.[11] (Adapted from Ref. 1).
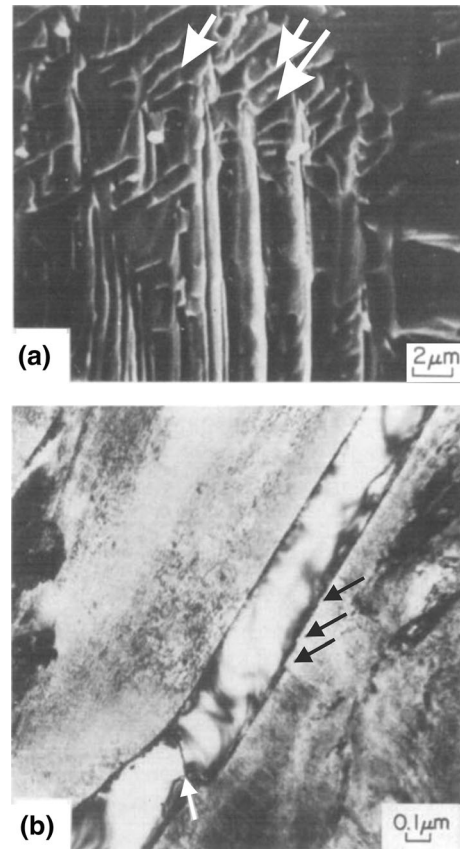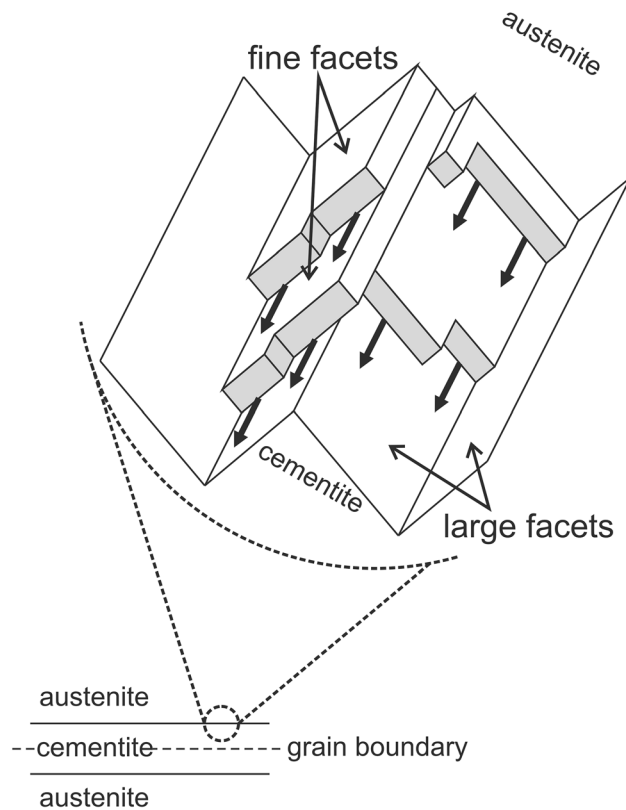
Fig. 5—Schematic representation of the austenite/cementite interface with large partially coherent facets and smaller incoherent mobile facets.

reported interledge spacing was approximately 200 times wider than for Widmanstätten cementite. They also explained that the used SEM techniques by Ando and Krauss[12] would be insufficient to observe the fine facets and that these cannot be revealed in the TEM micrographs due to the blurring effect of martensitic transformation during quenching. The justification of ledgewise growth by Ando and Krauss[12] relies, therefore, primarily on the observation of large ledges occupying habit planes at the austenite/cementite interface, i.e., analogous to the growth process of both types of proeutectoid cementite: grain boundary allotriomorphs and Widmanstätten precipitates.[1]

Ando and Krauss[12] subsequently used the theory for diffusion-controlled migration of ledges by Jones and Trivedi[22] to link grain boundary cementite thickening kinetics to the stepped morphology of the austenite/cementite phase boundary. They noted that their experimental kinetic results for AISI 52,100 steels were consistent with an increase of the interledge spacing with time and, thus, concluded that the sluggish thickening rate was likely resulting from a reduction in the lateral velocity of ledge motion instead of a change in the ledge nucleation rate.[12] In their critical response, Spanos et al.,[1] however, noted that Ando and Krauss's idea lacked a time-dependent description of the evolution of interledge spacing. In consideration of this drawback, Spanos et al.[1] used the following equation, first presented by Cahn et al.,[21] for lateral migration of ledges:

$$G_L = \frac{h}{\lambda} V_S,\qquad [4]$$

with G_L the cementite thickening rate, h the height of large ledges, λ the interledge spacing, and V_S the lateral ledge velocity. From Eq. [4], it can be further suggested that the previously mentioned interfacial structure barrier to growth, i.e., small G_L, has to manifest in small values of h/λ, assuming h constant. They then used the steady-state model of Atkinson for diffusionally interacting ledges[30,31] and the experimental results of Heckel and Paxton[11] to describe the corresponding time evolution of λ. For the considered alloy, at long reaction times, λ became significantly larger than the austenite grain size,[1] implying that the sluggish growth resulted in fact from a strong decrease of the ledge nucleation rate over time. Spanos et al.[1] finally considered, following the lack of success of the Vandermeer kinetic model, that further refinements of growth models based on disordered austenite/cementite phase boundaries "may be counterproductive" and suggested that accurate growth models must account for the ledgewise nature of the interface movement. The main question for a correct description of reaction kinetics would, thus, concentrate on the link between h and λ with time and temperature.

Several studies by the group of Spanos and Kral[5,7,32] followed after the work of Spanos et al.,[1] documenting the 3D morphology of grain boundary cementite in an alloy with composition Fe bal.–1.34C–13.1Mn (wt pct). In these studies, it was reported that the cementite grain boundary systematically represents a dendritic structure. The dendrite arms grow along the austenite grain boundary and do not extend into the grain beyond the previously described thickening process. The resulting classification of cementite precipitates thus turned out to be simpler than proposed by Heckel and Paxton[19] since only a single type of cementite grain boundary precipitate seemed to exist: the grain boundary cementite dendrite.[5,7] Previous reports of intragranular cementite precipitates were probably due to 2D sectioning effects.[7] Unfortunately, these studies[5,7,32] did not give additional information on the thickening process of grain boundary cementite. They suggested, however, the formation scheme of the cementite film as follows. The dendrites nucleate at the austenite grain edges and corners, grow along the grain edges before propagating along the grain boundaries (Figure 6(a)), and eventually impinge with other dendrites to form the cementite film (Figure 6(b)).[6,7] The thickening of the cementite film only occurs after the dendrites are impinged, which explains the mostly continuous cementite network at the austenite grain boundaries, which had been documented even at early reaction stages.[11,12,19]

C. Inspirations from Previous Studies

The work of Ando and Krauss[12] emphasizes the necessity to assess two different empiric parameters when interpreting experimental results on grain boundary cementite growth:
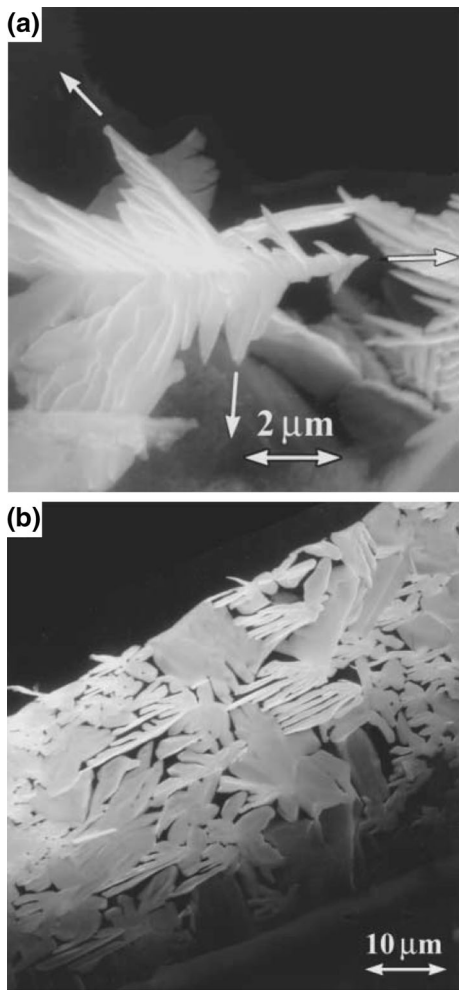
Fig. 6—SEM micrographs of grain boundary cementite in deep etched isothermally transformed samples. The morphology and growth directions along a grain edge (*a*) and impinged dendrites forming a grain boundary film (*b*) are shown. (Reprinted with permission from Ref. 7).

(1) The final cementite thickness depends on the proeutectoid cementite equilibrium fraction and the grain size in the case of purely diffusion-controlled growth. It should be noted that—more realistic—the existence of an interfacial structure barrier to growth, as suggested by Spanos *et al.*,[1,6] may stop the formation of new ledges and associated growth stops before the equilibrium cementite thickness is reached.

(2) The thickening rate depends on the diffusion and partitioning of the different alloying elements and the existence of the interfacial structure barrier to growth influencing the nucleation rate of ledges.

This means that accurately measured thickness data are required for different alloys and thermal treatments to serve as appropriate validation parameters for the modeling. The only published experimental data—to this day—on cementite thickening kinetics, where the actual measurement points are given, apply to Fe–C with minor alloying of Ni, and Fe bal.–1.20C–0.91Mn–0.23Si (wt.pct) steels by Heckel and Paxton[11] at 800 °C. This makes these two the only usable datasets in the literature for unbiased assessments of new kinetic models.

It should be noted that determination of experimental thickness over a logarithmic time scale instead of a linear is advisable (and indicated by Eq. [3]) to distinguish between sluggish growth and growth stop. Appropriate conversion from 2D measurements to 3D data is also important but will be addressed in the next chapter.

It is concluded from the present literature review that no predictive model of grain boundary cementite thickening kinetics is available yet. The latest kinetic work by Spanos *et al.*[1] only interprets a posteriori the experimentally measured sluggish growth. As mentioned previously, the major issue is determining properly the ledge height and interledge spacing as functions of time, temperature, and chemical composition. Small values of h/λ could be seen as the symptoms of an interfacial structure barrier to growth,[1,6] however, no physical explanation of its nature is given. A likely hypothesis concerns the existence of elastic interactions between ledges due to differences in molar volumes of austenite and cementite, preventing new ledge formation when the longitudinal growth front of previously nucleated ledges is too close to the nucleation site, as suggested for austenite-to-ferrite transformations by Chen *et al.*[27] However, to the authors' knowledge, such elastic interactions between ledges have not yet been experimentally observed and reported.

The ambiguous situation requires in-depth reconsideration of modeling of cementite growth involving the model assessment by validation with the most suitable, interpretable experimental data, as discussed above. We consider two modeling strategies for grain boundary cementite growth. The first one considers recent work on integrated modeling of solid-state nucleation and growth of precipitates[13–16,33] based on the thermodynamic extremum principle of maximum rate of entropy production.[34] The corresponding model formulation is based on the diffusional growth of precipitates arranged along grain boundaries, which appears to be representative of secondary cementite growth. The second strategy tests the modeling of ledgewise growth and the presumption of the existence of an interfacial structure barrier to growth, where particular focus lies on its energetic formulation and time evolution. Both strategies will be evaluated using the experimental data of Heckel and Paxton for almost pure Fe–C hypereutectoid steel at 800 °C,[11] heat-treated such as to prevent Widmanstätten cementite formation, in order to assess the evolution of grain boundary cementite alone with only minimum influence of substitutional alloying elements.

III. CONVENTIONAL NUCLEATION AND GROWTH APPROACH

A. Methodology

1. Precipitation modeling

This approach considers the formation of a grain boundary cementite film with a homogeneous thickness in a mean-field approximation as a precipitation reaction occurring at the austenite grain boundaries where the grain boundary cementite network develops over all grain boundaries. These hypotheses are similar to those made by Heckel and Paxton[11] and seem reasonable for a hypereutectoid steel with little amount of discontinuities in its cementite network, as it was observed in all investigated steels of Ref. 11. Furthermore, this approach assumes that the time evolution of the grain boundary cementite phase fraction for the real film thickening and the simulated precipitates' nucleation and growth is similar. This allows linking d the cementite half-thickness to f_{SC} the proeutectoid cementite phase fraction, given that no Widmanstätten cementite is present in the investigated microstructure:

$$d = \frac{f_{SC} V}{2 A_{GB}}, \qquad [5]$$

with V the volume of the system and A_{GB} the total grain boundary area. In the present modeling approach, grains have the geometry of equiaxed tetrakaidecahedra, and the calculation of A_{GB} is explained in Ref. 33. Accurate modeling of f_{SC} requires the proper definition of the diffusion field for the bulk carbon diffusion from the grain interior to the precipitates and needs to take into account the fast short-circuit grain boundary diffusion. For this, a model for growth and coarsening of grain boundary precipitates with conical diffusion fields developed by Kozeschnik et al.[13] and implemented in the software MatCalc is utilized. Its mathematical formalism uses the thermodynamic extremum principle, first formulated by Onsager,[34,35] demonstrated to represent a useful modeling tool by Svoboda et al.,[36] and subsequently building the foundation for the evolution equations describing the size and chemical composition evolution of precipitates in the SFFK (Svoboda–Fischer–Fratzl–Kozeschnik) model.[14–16] Figure 7 compares the present simulation setup to the one with cementite film growth over spherical grains used in the Heckel and Paxton model, the Vandermeer model, or in Dictra simulations. More specifically, the present approach defines conical bulk diffusion fields from the center of the tetrakaidecahedral grain to a grain boundary region surrounding each precipitate and short-circuit diffusion along the grain boundaries by the use of a pre-factor to the diffusion activation energy (Figure 7(a)).[13] Such an approach applies experimentally and theoretically assessed dependencies of the precipitate coarsening on temperature and grain size. This approach differs from the classical diffusion approach used in the previous models or in Dictra[37] where no precipitate and no nucleation event are described, the grain is spherical, and the system is centrally symmetric, see Figure 7(b).
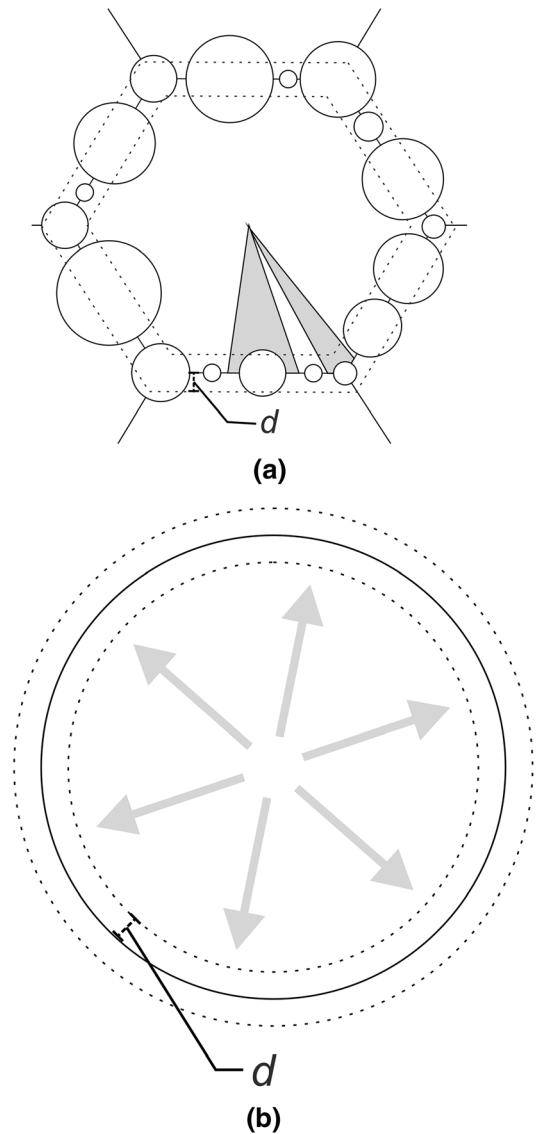
(a)

(b)

Fig. 7—Schematic precipitate distribution, diffusion fields (gray areas), and mean film half-thickness d for precipitation at grain boundaries in 2D (a) compared to the diffusion geometry (gray arrows) for film growth over a spherical grain (b).

Nucleation kinetics is simulated with classical nucleation theory (CNT), where the transient nucleation rate J is given as[16]

$$J = N Z \beta^* exp\left(\frac{-G^*}{k_B T}\right) exp\left(\frac{-\tau}{t}\right), \qquad [6]$$

with N being the number of potential nucleation sites, Z the Zeldovich factor, β^* the atomic attachment rate, G^* the critical nucleation energy, k_B the Boltzmann constant, T the absolute temperature, and τ the incubation time. The calculation methods of Z, β^*, and τ are presented in detail in References 16 and 33 J represents the number of nuclei created per unit volume and time. The critical nucleation energy G^* is calculated from the extremum value of ΔG_{nucl} for heterogeneous precipitation at grain boundaries, which has

recently been reported by Miesenberger et al.,[38] by the expression:

$$\Delta G_{nucl} = \frac{4}{3}\pi\rho^3\Delta G_{vol} + 4\pi\rho^2\gamma - \Delta G_{het}, \qquad [7]$$

where ΔG_{vol} is the volume free energy change and γ is the precipitate/matrix interfacial energy. γ is calculated from the Generalized Broken Bond model developed by Sonderegger and Kozeschnik.[39,40] ΔG_{het} is the energy gain at the nucleation site due to partial replacement of the original grain boundary area by the nucleus volume. This effect reduces the value of ΔG_{nucl} at heterogeneous nucleation sites, thus making nucleation energetically more favorable. The value of ΔG_{het} depends on the nucleus radius ρ and grain boundary energy γ_{GB}, with $\Delta G_{het,gb} = \pi\rho^2\gamma_{GB}$.[38] In contrast to Classical Nucleation Theory, the values for the critical nucleation radius and critical nucleation energy based on Eq. [7] must be sought numerically.

2. Simulation setup

The alloy considered in the present simulations is Steel F from Heckel and Paxton,[11] with the composition given in Table I.

The Si and Mn concentrations are low enough such that they are ignored in the simulation. The simulated steel is thus considered as Fe bal.–1.16C–0.03Ni (wt. pct). The reported austenite grain size by Heckel and Paxton was ASTM − 1 to 0. In the present work, an average of both grain sizes is used in our simulation, corresponding to a 600 μm grain diameter, as Heckel and Paxton did in their work. The reaction temperature is 800 °C. The precipitates are considered to have spherical shape, and the nucleus chemical composition is determined by the criterion of ortho-equilibrium (maximum chemical driving force).

For better reading and easier comparison to the experimental results, we plot the evolution of d with time using $t = 0$ as the time of cementite nucleation, similarly as Heckel and Paxton[11] as well as Spanos et al.[1] This does not mean that we do not simulate nucleation, but only that the simulation results of d are drawn starting from the cementite nucleation time. MatCalc is used first to simulate the isothermal grain boundary cementite evolution, in order to validate it by experimental data. Simulation results are compared to Vandermeer's simulation[1] as well as to a moving phase boundary solution realized in the software Dictra (version 2021b). The Dictra simulation considered the growth of a cementite film covering an austenite sphere, with the same composition as in the MatCalc simulation, using the TCFE11 thermodynamic and MOBFE6 diffusion databases. We then investigate the influence of the Ni concentration c_{Ni} and the choice of diffusion field

geometry on the simulated growth kinetics. We finally present the calculated isothermal time–temperature–precipitation (TTP) and continuous cooling precipitation (CCP) diagram for proeutectoid cementite in the Steel F between 900 °C and 750 °C, yielding additional "virtual experiment" information on cementite growth kinetics at various temperatures.

For our MatCalc simulations, Calphad-assessed Gibbs energies and diffusivities are taken from the open MatCalc databases mc_fe.tdb (release 2.060) and mc_fe.ddb (release 2.012), respectively. The cementite/austenite interfacial energy γ_{cem} is calculated from the Generalized Broken Bond model[39,40] using the same databases. The default value in MatCalc of grain boundary energy γ_{GB} is used. The adjusted, i.e., freely selectable, and evaluated, i.e., given by MatCalc, simulation input parameters are summarized in Table II.

3. 2D/3D conversion of experimental measurements

For geometrical reasons, measurements of the average grain boundary cementite thickness with a two-dimensional micrograph overestimate its real value in 3D. Heckel and Paxton[11] treated this problem by assuming spherical grains and "disc-like shape" for the grain boundary films and using an expression derived by Fullman[41]:

$$d_{2D} = 2d, \qquad [8]$$

with d_{2D} the mean film half-thickness measured linearly on the micrograph. However, the application of this approach seems critical in the case of grain boundary cementite because Fullman's expression[41] applies to the calculation of the thickness of circular plates, not of the thickness of a film surrounding them. We use an alternative 2D/3D conversion approach in the present work. It is based on the integration of the grain boundary film thickness over the quarter of a circle's perimeter under the prerequisite that the circle has the same radius as the spherical grain and the normal film half-thickness is constant over the circle perimeter. This leads to the following expression:

$$d_{2D} = \frac{2}{\pi}\int_0^{\frac{\pi}{2}}\left((R+d)\cos\left(\sin^{-1}\frac{R\sin\theta}{R+d}\right) - R\cos\theta\right)d\theta, \qquad [9]$$

Table II. Adjusted (ad.) and Evaluated (ev.) Simulation Parameters

Grain size (μm)	600	ad
Nucleation sites	grain boundaries	ad
Heterogeneous site energy	$\pi\rho^2\gamma_{GB}$	ad
Interfacial energy γ_{cem} (J/m^2)	0.0728	ev
Grain boundary energy γ_{GB} (J/m^2)	0.5	ev
C diffusivity in austenite at 800 °C (m^2/s)	3.33 .10^{-12}	ev
Driving force for cementite nucleation (J/mol)	556	ev

Table I. Experimental Steel Composition in Weight Percent

C	Ni	Si	Mn
1.16	0.03	0.001	< 0.001

d_{2D} and R are supposed to be known values, and d is the unknown parameter. The derivation of Eq. [9] is detailed in the appendix. The integral at the right-hand side of Eq. [9] can only be solved numerically. Therefore, the calculation algorithm searches iteratively for the value of d, leading to the nearest possible derived value of d_{2D} to the input value of d_{2D}. The present 2D/3D conversion approach will be designated henceforth as "integration approach." We will compare our simulated grain boundary cementite thickness to Heckel and Paxton's experimental data treated by both Fullman's approach and the integration approach in the following.

B. Results

1. Isothermal aging

The present approach based on nucleation and growth of grain boundary cementite precipitates matches significantly better the experimental data than the published results of the Vandermeer model and the Dictra simulation, as shown in Figure 8 for isothermal aging at 800 °C. This observation is valid with the Fullman's and the integration approach for 2D/3D conversion of the experimental data. After approximately 5000 s, however, the simulated growth becomes faster than in the experiment, and the simulated value of d overestimates the experimental half-thickness. The evolution of d over time shows a similar S-shaped curve as both other models, but with a delay. Furthermore, at the end of the reaction, the simulated film half-thickness reaches an equilibrium value (3.30 μm) similar to the one predicted by the Dictra simulation (3.51 μm) and close to the final cementite half-thickness predicted by the Vandermeer model (3.15 μm). However, in our simulation, equilibrium is reached after approximately 4 10^5 s, which is about 4 and 10 times later than with Dictra and the Vandermeer model, respectively. Our

simulation, thus, seems to contradict the prediction of Ando and Krauss[12] that the thickening of cementite effectively stops before reaching the equilibrium thickness. We note that the experimental data from Heckel and Paxton for Steel F does not indicate growth stop during their experiment.

The Ni concentration strongly influences the kinetics of d, even at low values (Figure 9(a)). The lower the Ni concentration, the earlier starts cementite nucleation, and the higher is the density of precipitate nuclei (Figure 9(b)). Up to 0.01 wt pct Ni, an order of magnitude difference in the Ni concentration leads to a difference of approximately an order of magnitude in the simulated cementite nucleation time (Table III). On the other hand, with 0.03 wt pct Ni, the diffusion field geometry does not influence the cementite nucleation time (Table III). However, spherical diffusion fields lead to a much faster precipitate growth (Figure 9(c)), even faster than with Dictra or the Vandermeer model, and to a higher precipitate number density (Figure 9(d)). This shows the crucial role of the appropriate diffusion field model for the sound simulative prediction of heterogeneous precipitation.

2. Isothermal and continuous cooling time–temperature–precipitation computations

Figure 10 presents fully predictive computation results of isothermal and continuous time–temperature–precipitation for steel Fe bal.–1.16C–0.03Ni (wt pct). For easier comparison to experiments, the simulated TTP and CCP diagrams (Figure 10) represent proeutectoid cementite growth in terms of half-thickness d. One can find from Figure 10a that, during isothermal transformation, the larger the cementite half-thickness or phase fraction is, the lower is the maximum temperature allowing to reach it, which is consistent with the increase of the equilibrium proeutectoid cementite phase fraction with decreasing temperature between the A_{CM} and eutectoid temperatures in the Fe–C phase diagram. Once more, one also notes the particularly low thickening rate of cementite during isothermal transformations, since, for all considered temperatures, at least 10^4 s are necessary to reach about 3 μm film half-thickness for the Steel F alloy.

The CCP diagram (Figure 10(b)) shows the strong effect of cooling rates on the cementite thickness, with higher cooling rates strongly limiting cementite growth. 0.01 K/s cooling rate leads to a simulated cementite half-thickness above 1 μm, whereas cooling rates above 1 K/s result in lower values of the final half-thickness close to 0.1 μm.

C. Discussion

1. Simulation background

Firstly, we are aware that, taking grain boundaries as potential nucleation sites is a simplification for the nucleation sites observed in experiment for grain boundary cementite, specifically grain boundary edges and corners.[5,6] However, Heckel and Paxton reported that cementite already covered the entire grain boundary network at the early stages of growth.[11,19] It seems,
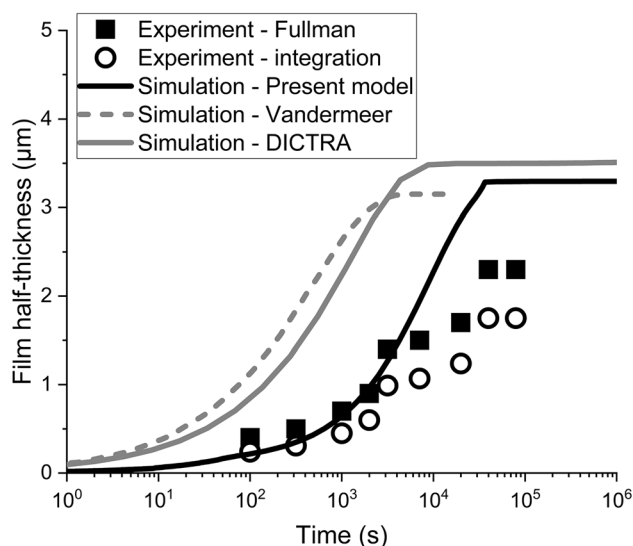
Fig. 8—Comparison between the simulated cementite half-thickness by the classical nucleation and growth model with the simulation by Dictra and the Vandermeer model[1] and the experimental data from Heckel and Paxton[11], treated by the Fullman approach and the integration approach.
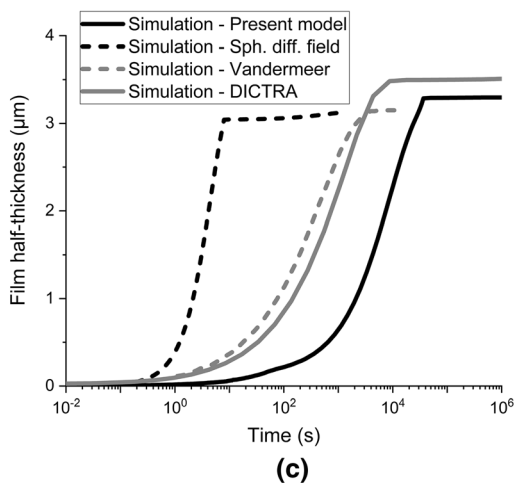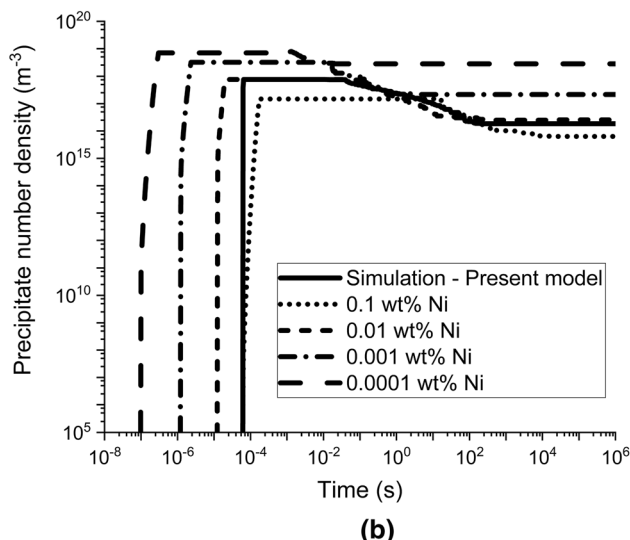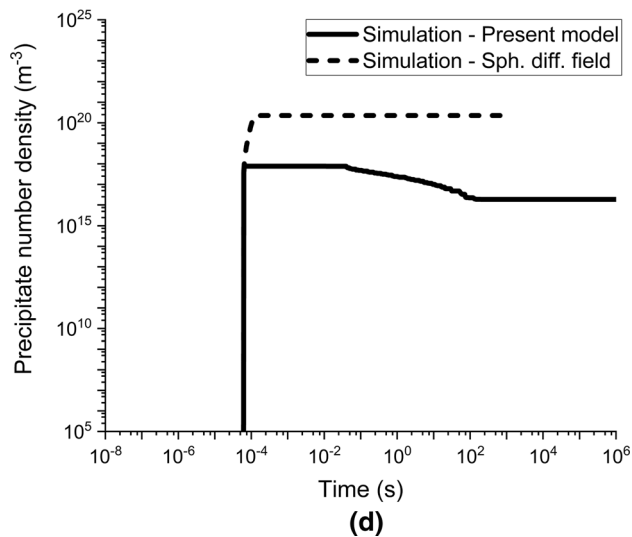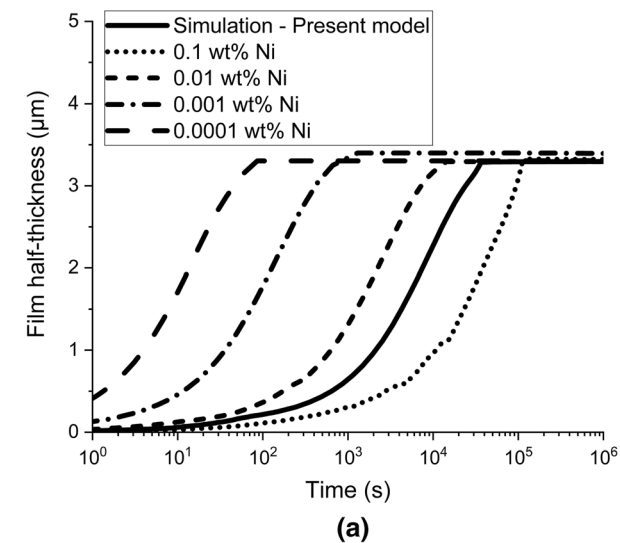
(a)

(b)

(c)

(d)

Fig. 9—continued.

Fig. 9—Simulated cementite half-thickness and precipitate number density for different Ni concentrations (*a*, *b*) and with or without spherical diffusion field to the precipitates (*c*, *d*).

thus, a reasonable approximation to simulate a grain boundary cementite film by many spherical cementite precipitates nucleating over the whole grain boundary

and eventually impinging. In other words, our simulation does not take into account the very early nucleation stage because "transferring" nucleated cementite at edges and corners to observed cementite network in the simulation is unnecessarily demanding for the assessment of principle feasibility of the modeling approach presented here.

In addition, the validity of Eq. [5] is straightforward only for a continuous grain boundary cementite network and in the absence of Widmanstätten precipitates. Additional work would have to take into account the respective weight of grain boundary and Widmanstätten cementite in f_{SC}, as well as the formation of discontinuities in the cementite film, present in particular in steels with substitutional alloying elements.

The assumption of the cementite film representation by cementite grain boundary precipitates is justified because the maximal precipitate number density is reached very early in the simulation (Figure 9(b)), and the grain boundary as nucleation site becomes saturated with cementite nuclei after only short reaction times. This is further important for justifying the derivation of ΔG_{het} for spherical precipitates, although spheres do not occupy the same fraction of grain boundary area as a film.

2. *Validation of kinetic simulations*

The present modeling approach shows that simulation of the grain boundary cementite thickening kinetics is possible using diffusion control of the reaction and without accounting for ordering effects at the austenite/cementite interface, at least at early reaction times, despite the suggestion by Spanos *et al.*[1] to abandon this modeling strategy. The fundamental difference between our model and the other simulations available (Vandermeer model, Dictra) is that we take into account the conditions of the nucleation of the cementite phase and the conical geometry of the diffusion field from the grain to a grain boundary precipitate with the grain boundary collector plate mechanism. One would expect our

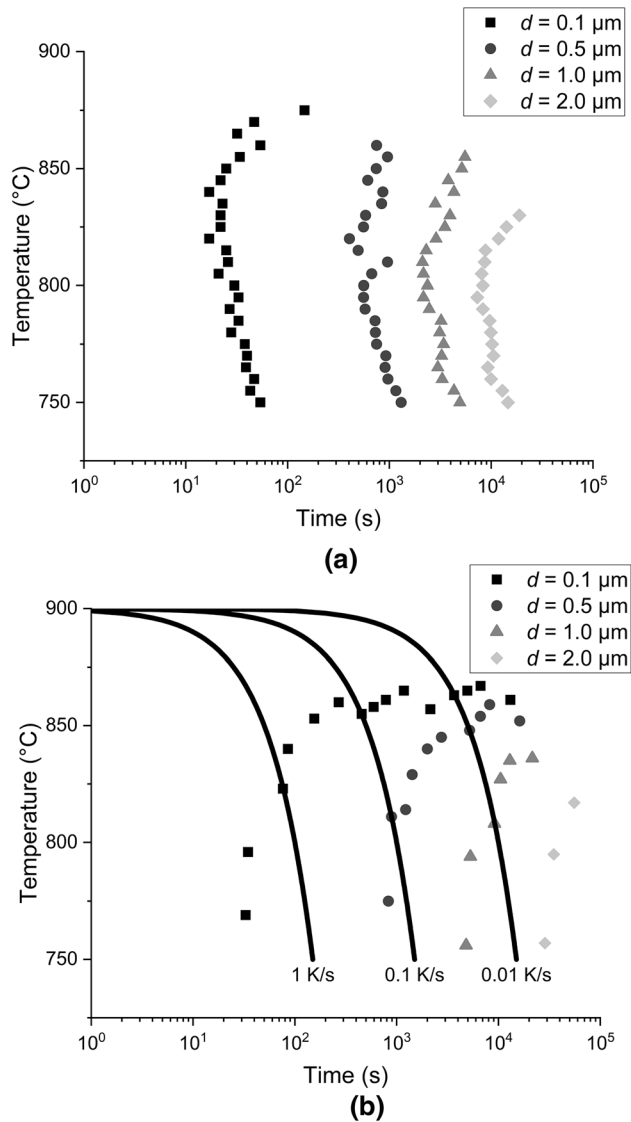| Present model—conical diffusion field, $c_{Ni} = 0.03$ | | Spherical diffusion field, $c_{Ni} = 0.03$ | |
$6.10 \cdot 10^{-5}$ s		$6.10 \cdot 10^{-5}$ s	
$c_{Ni} = 0.1$	$c_{Ni} = 0.01$	$c_{Ni} = 0.001$	$c_{Ni} = 0.0001$
$6.10 \cdot 10^{-5}$ s	$1.22 \cdot 10^{-5}$ s	$1.20 \cdot 10^{-6}$ s	$9.77 \cdot 10^{-8}$ s

Fig. 10—Simulated isothermal TTP (*a*) and CCP (*b*) diagram for proeutectoid cementite in the Steel F alloy.

depending on their number density. These parameters, thus, appear particularly important for the modeling of cementite thickening kinetics. It is important to note that the lack of incubation time for cementite nucleation in the Vandermeer or Dictra models cannot possibly be the sole reason for their difference with our simulation. The incubation time would need to be of the order of magnitude of 10^1 s if it was the case (Figure 8), which is unrealistically higher than the values in Table III, and the Vandermeer and Dictra simulations would need in addition a correspondingly reduced growth rate at all reaction times to keep the correct slope in Figure 8 due to the logarithmic time scale. We note, however, that the larger difference between our simulation and the experiment at late reaction times may indicate the increasing importance of an additional controlling mechanism over time, for example, local elastic effects due to the presence of cementite ledges.[26]

The retarding influence of Ni on nucleation and growth of proeutectoid cementite (Figure 9(a), (b)) is consistent with the low solubility of Ni in the cementite phase, making Ni partitioning at the grain boundary necessary for cementite formation. However, further assessment of the large influence of variations—even within low values—of the concentration of substitutional alloying elements, such as Ni, is necessary for an in-depth understanding of their effect on cementite growth kinetics and, therefore, for applicability of the present model to industrial alloys. This can be done by comparing the present model and experimental results regarding more complex multi-component systems.

The present simulation contradicts the observations by Ando and Krauss[12] of final experimental thicknesses significantly lower than the equilibrium thickness. However, Ando and Krauss made these observations only for their industrial AISI 52,100 steels—which contain significant amounts of Cr, Mn, or Si, among other elements—and with linear time scale (Figure 2(a)). In order to solve this question, experiments with longer annealing times would be necessary, where stoppage of cementite thickening would be noticeable in a logarithmic time scale.

The simulated TTP diagram (Figure 10(a)) reveals again, after the observations by Ando and Krauss,[12] that a logarithmic time scale is more appropriate than a linear time scale for the description of grain boundary cementite thickening. Even though cementite starts to form very early (Figure 9(b)), it needs hours of isothermal treatment to reach half-thickness values over 1 μm for any considered temperature. Similarly, for the

simulation with a conical diffusion field to give results close to the ones of the Dictra simulation due to their similarities. However, the model by Kozeschnik *et al.* for the growth of precipitates at grain boundaries[13] takes well into account not only the amount of available carbon for the cementite growth but also the faster diffusion path along the grain boundaries and the local growth conditions of all cementite precipitates

continuous cooling simulations, additional experimental data for the same alloy would be useful to assess the accuracy of the diagram.

3. From conventional modeling to ledgewise growth consideration

The conventional nucleation and growth approach does not explicitly describe the formation of ledges at the austenite/cementite interface. It contains no thermodynamic description of the interfacial structure barrier to growth suggested by Spanos et al.[1,6] either. Its only thermodynamic equivalent to a change in the reaction conditions at the interface is ΔG_{het}, which makes cementite nucleation at the austenite grain boundary more favorable when the reaction advances. However, it tells nothing about the potential autocatalytic nucleation of cementite over existing cementite. If the present model of grain boundary cementite thickening would be physically correct and sufficient, this would also mean that ledges represent morphological features of the austenite/cementite interface that play no role in the kinetics of the reaction. However, we would need to find another reason and associated adaption of the present modeling to account for the particularly slow growth of proeutectoid cementite, especially at late reaction times where the conventional nucleation and growth approach overestimates the cementite thickening rate. In the following, the alternative view of a stepped austenite/cementite interface and its suitability for a complete picture of the austenite to cementite transformation is assessed.

IV. AUTOCATALYTIC LEDGE NUCLEATION APPROACH

A. Methodology

The present second approach is based on the observations by Ando and Krauss[12] on the stepped morphology of the austenite/cementite interface and the assumptions of Spanos et al.[1] on the kinetic role of the ledge nucleation rate. Here, we establish a phenomenological time-dependent description of the interfacial structure barrier to growth[1,6] before equilibrium. We assume that the cementite ledge nucleation rate controls the grain boundary film thickening kinetics and that all cementite ledges have the same ledge height h. The cementite half-thickening rate G_L becomes then

$$G_L(t) = h N_L(t), \qquad [10]$$

with N_L being the ledge nucleation rate. Both G_L and N_L are functions of time, and N_L follows an Arrhenius expression:

$$N_L(t) = N_{L0} \exp\left(\frac{-E_{eff}(t)}{k_B T}\right), \qquad [11]$$

with N_{L0} being the ledge nucleation rate at $t = 0$ and E_{eff} a phenomenological time-dependent effective energy barrier including all local physical mechanisms

restraining the nucleation of new ledges over time. This means first the availability of carbon near the reaction front, here detached from the total carbon availability in the system, thus allowing this model to describe the evolution of d only preceding equilibrium; this also means the energetic cost of the creation of an ordered austenite/cementite interface with its corresponding crystallographic constraints and the atomic coherency varying with the interface orientation (see chapter 2.2); this finally means the potential elastic interactions between ledges due to the change in molar volume inhibiting ledge nucleation as suggested by Chen et al.[27]

We define $t = 0$ as the moment of nucleation of cementite, that is the moment of nucleation of the first ledge at the considered nucleation site. Thus, per definition, $N_{L0} = 1/\tau_0$ with τ_0 being the incubation time for the first ledge. The following point is to deduce an expression of E_{eff}. We suggest the following:

$$E_{eff}(t) = \alpha \ln\left(\frac{t}{\tau_0} + 1\right), \qquad [12]$$

with α being an energy factor depending on the alloy composition and the reaction temperature. Equation [12] shows that $E_{eff}(t = 0) = 0$, which means that E_{eff} is a relative value to $t = 0$. Combining Eqs. [10] through [12] gives an expression of G_L as a function of time, and d follows as the integral of G_L over t, with $d(t = 0) = h$:

$$d(t) = \frac{h k_B T \left(\left(\frac{t}{\tau_0} + 1\right)^{1 - \frac{\alpha}{k_B T}} - 1\right)}{k_B T - \alpha} + h, \qquad [13]$$

We use $h = 7$ nm to assess the present approach for the Steel F alloy by Heckel and Paxton,[11] following the observations by Spanos and Aaronson on the large ledges of the austenite/cementite interface.[42] The values of α and τ_0 will be fitted using the least square method and Eqs. [12] and [13], from values of E_{eff} derived from the experimental data of d using Eqs. [10] and [11]. The experimental value of G_L at the ith experimental time step (used in Eq. [10] for the derivation of the experimental E_{eff}) is derived as the slope between the $(i$-1)th and $(i + 1)$th experimental values of d. Both, the Fullman and the integration approaches, are considered for 2D/3D conversion of experimental data, see 3.1.3. The obtained values of τ_0 will then be compared to the one calculated in the classical nucleation and growth approach at early reaction times.

B. Results

The present phenomenological approach provides a good fit of experimental data for the Steel F system by Heckel and Paxton at experimentally and industrially relevant reactions times, see Figure 11. At later reaction times than the latest experimental data, d diverges. No stop of cementite thickening occurs with this approach. Equation [12] fits very well the experimental evolution of E_{eff} (Figure 12), and this fit of data treated by the
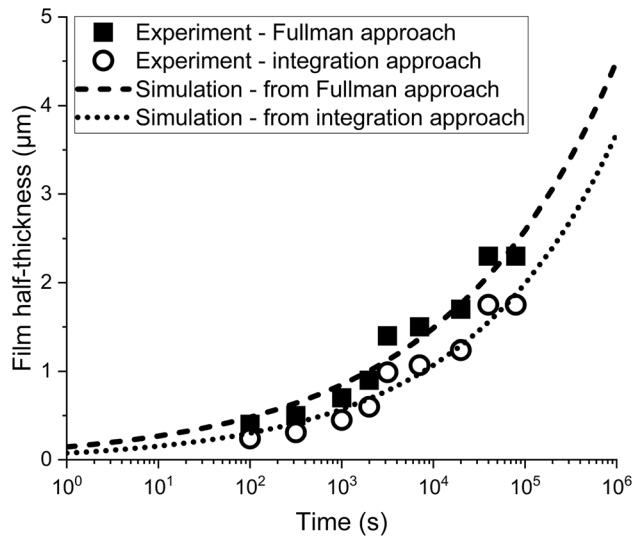
Fig. 11—Comparison between the simulated cementite half-thickness by the ledge nucleation control model with the experimental data from Heckel and Paxton,[11] treated by the Fullman approach and the integration approach.
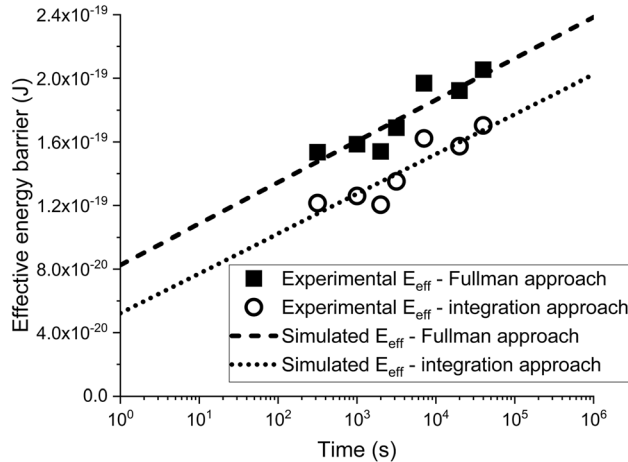

Fig. 12—Simulated and experimental evolution of E_{eff} obtained from data treated by the Fullman approach and the integration approach.

Fullman approach or by the integration approach yields the values of α and τ_0 shown in Table IV. The value of α fitted from the Fullman approach is slightly higher than that obtained from the integration approach. However, their relative difference is only less than 4 pct. On the other hand, τ_0 obtained from the integration approach data is one order of magnitude higher than its value from the Fullman approach data. Both values of τ_0 are several orders of magnitude higher than τ_0 obtained from the MatCalc calculation, considering conventional nucleation of spherical precipitates. E_{eff} is in the order of magnitude 10^{-19} J at the considered reaction times.

C. Discussion

The present model fits the experimental data and thus the cementite growth rate for the Steel F system by Heckel and Paxton[11] more accurately than the previous

Table IV. Coefficients α and τ_0 Fitted from the Experimental Data Treated by the Fullman Approach and the Integration Approach, and Value of τ_0 Simulated in MatCalc

From Fullman approach		From integration approach		From MatCalc
α (J)	τ_0 (s)	α (J)	τ_0 (s)	τ_0 (s)
1.13. 10^{-20}	6.63. 10^{-4}	1.09. 10^{-20}	8.26. 10^{-3}	6.10. 10^{-5}

precipitation simulation approach in the industrially and experimentally relevant time range. E_{eff} with Eq. [12] gives an accurate energetic description of the relative evolution of the interfacial structure barrier to growth. The derived values of α and τ_0 from both considered sets of experimental data are consistent with each other: the experimental values of d are lower when treated by the integration approach than by the Fullman approach, which translates into a larger ledge incubation time. Even though the difference between τ_0 considering ledge nucleation and conventional nucleation (see Table IV) appear huge, this can be easily explained: it is realistic that the incubation time for the formation of a 7-nm-high ledge is larger than for a spherical nucleus for which the mean radius at the earliest precipitation stages is barely one nanometer.

We implicitly assumed for the treatment of the available experimental data that the ledge nucleation rate N_L is the same for all cementite nucleation sites and that the grain boundary film thickness is thus homogeneous. The reason is that the data for Steel F are average of the film thickness over the whole microstructure and do not consequently report variations of the thickness over the grain boundary. However, one could redefine N_L as the ledge nucleation rate for a given nucleation site without changing the rest of the modeling approach. Our approach would then allow describing variations in the film thickness from different nucleation sites for a given time step and their associated variations of α and τ_0. There is, unfortunately, still a lack of available quantitative experimental data on this subject for the moment.

An important limitation of the present approach is the limited physicality of E_{eff} due to its phenomenological nature. Equation [12] proposes a time-dependent expression of an effective energy barrier to ledge nucleation, allowing only to describe—not predict—the evolution of the reaction rate during the phase transformation. There is no distinction within E_{eff} between the influences of the different physical factors affecting cementite thickening and Eqs. [11] through [13] are valid only while growth commences. Consequently, this approach does not contain any thermodynamic control of the cementite growth and, thus, does not consider any maximal value of the cementite thickness in its present form. A physical description of the factors α and τ_0 will be necessary for successful predictions of cementite thickening kinetics, taking into account the morphology of the austenite/cementite interface. We suggest α to be

mainly influenced, among the parameters listed in chapter 4.1, by the evolution of local carbon concentration and the elastic interactions among ledges, since they would affect the conditions of ledge production over time, whereas the crystallographic constraints due to atomic mismatch would express already at the formation of the first ledge, thus influencing τ_0.

V. CONCLUSIONS

We investigate two modeling approaches for the thickening kinetics of grain boundary cementite. The first one is based on the SFFK model for nucleation and growth of cementite precipitates on the austenite grain boundary, whereas the second assumes control of the cementite film thickness by the ledge nucleation rate expressed by a time-dependent effective energy barrier to nucleation. Both approaches deliver significantly improved results compared to all previously published models for an Fe–C hypereutectoid alloy. These results demonstrate that accurate modeling of cementite thickening kinetics does not necessarily require a description of the ledge motion at the austenite/cementite interface. Ledge formation rate does not necessarily have to be the controlling parameter of cementite thickening. However, a simple phenomenological description of its time evolution allows for a rather accurate simulation of the reaction kinetics before reaching equilibrium. Linking ledge nucleation and movement to its controlling thermodynamic and thermokinetic parameters would not only allow to accurately describe the grain boundary cementite thickness but also to understand better the austenite/cementite interface evolution during the reaction, and, thus, the reason for local thickness variations or breaks in the continuity of the grain boundary cementite film.

CONFLICT OF INTEREST

On behalf of all authors, the corresponding author states that there is no conflict of interest.

OPEN ACCESS

APPENDIX

Derivation of Eq. [9].

We consider a spherical austenite grain of radius R surrounded by a cementite film of normal half-thickness d constant over the grain's surface. If we define an intersection plane corresponding to the sample's surface, we define δ the apparent grain boundary cementite half-thickness at the intersection plane. Due to its symmetries, the system's representation can be reduced to the intersected quarter of two two-dimensional concentric circles with center O, see Figure A1.

We define θ as the angle between the basis of the quarter circles and the austenite/cementite interface at the intersection plane. This means that δ is a function of θ and that the mean film half-thickness measured in the micrograph d_{2D} is the average of δ over $0 \leq \theta \leq \pi/2$:

$$d_{2D} = \frac{2}{\pi} \int_0^{\frac{\pi}{2}} \delta(\theta) d\theta. \qquad [A1]$$

H is the distance between the intersection plane and the basis of the quarter circles, and h is the distance
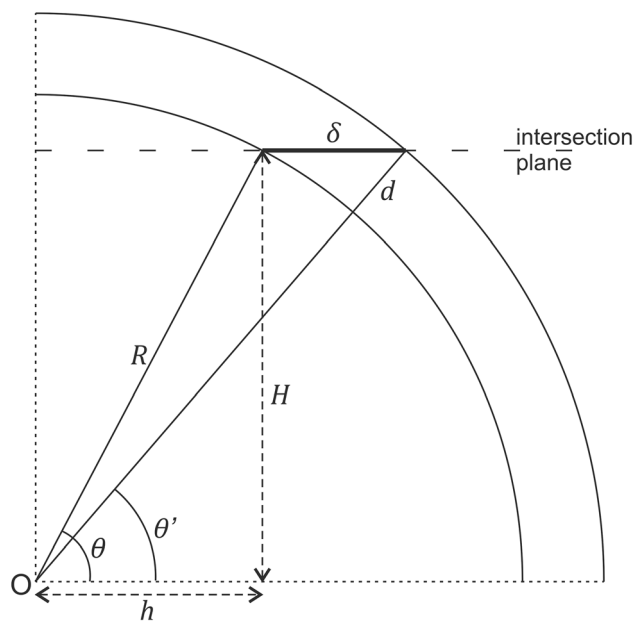

Fig. A1—Reduced schematic 2D representation of the austenite grain and cementite film geometry.

between O and the austenite/cementite interface at the intersection plane projected on the basis of the quarter circles. We also define θ' as the angle between the basis of the quarter circles and the surface of the cementite film at the intersection plane. We have then the following expressions:

$$H = R\sin\theta, \qquad [A2]$$

$$h = R\cos\theta, \qquad [A3]$$

$$\sin\theta' = \frac{H}{R+d} = \frac{R\sin\theta}{R+d}, \qquad [A4]$$

$$\cos\theta' = \frac{h + \delta(\theta)}{R+d} = \frac{R\cos\theta + \delta(\theta)}{R+d}. \qquad [A5]$$

Then, using Eqs. [A4] and [A5], we have

$$\delta(\theta) = (R+d)\cos\theta' - R\cos\theta$$
$$= (R+d)\cos\left(\sin^{-1}\frac{R\sin\theta}{R+d}\right) - R\cos\theta, \qquad [A6]$$

and we derive Eq. [9] by combining Eqs. [A1] and [A6].

REFERENCES

1. G. Spanos, W.T. Reynolds, and R.A. Vandermeer: *Metall. Trans. A*, 1991, vol. 22, pp. 1367–80.
2. Y.J. Li, P. Choi, S. Goto, C. Borchers, D. Raabe, and R. Kirchheim: *Acta Mater.*, 2012, vol. 60, pp. 4005–16.
3. R.K. Janutiene: *Mechanika*, 2016, vol. 22, pp. 432–37.
4. K. Ankit, A. Choudhury, C. Qin, S. Schulz, M. McDaniel, and B. Nestler: *Acta Mater.*, 2013, vol. 61, pp. 4245–53.
5. C.Y. Hung, G. Spanos, R.O. Rosenberg, and M.V. Kral: *Acta Mater.*, 2002, vol. 50, pp. 3781–88.
6. G. Spanos and M.V. Kral: *Int. Mater. Rev.*, 2009, vol. 54, pp. 19–47.
7. M.V. Kral and G. Spanos: *Acta Mater.*, 1999, vol. 47, pp. 711–24.
8. G.H. Zhang, J.Y. Chae, K.H. Kim, and D.W. Suh: *Mater. Charact.*, 2013, vol. 81, pp. 56–67.
9. C.Y. Han, T.D. Mottishaw, G.D.W. Smith, D.V. Edmonds, and A.G. Stacey: *Mater. Sci. Eng. A*, 1995, vol. 190, pp. 207–14.
10. G. Langford: *Metall. Trans. A*, 1977, vol. 8, pp. 861–75.
11. R.W. Heckel and H.W. Paxton: *Trans. Metall. Soc. AIME*, 1960, vol. 218, pp. 799–806.
12. T. Ando and G. Krauss: *Acta Metall.*, 1981, vol. 29, pp. 351–63.
13. E. Kozeschnik, J. Svoboda, R. Radis, and F.D. Fischer: *Model. Simul. Mater. Sci. Eng.*, 2010, vol. 18, 015011.
14. J. Svoboda, F.D. Fischer, P. Fratzl, and E. Kozeschnik: *Mater. Sci. Eng. A*, 2004, vol. 385, pp. 166–74.
15. E. Kozeschnik, J. Svoboda, P. Fratzl, and F.D. Fischer: *Mater. Sci. Eng. A*, 2004, vol. 385, pp. 157–65.
16. E. Kozeschnik: in *Encyclopedia of Materials: Metals and Alloys*, vol. 4, Elsevier, 2022, pp. 521–26.
17. J. Crank: *The Mathematics of Diffusion*, Clarendon Press, Oxford, 1975.
18. P. Gustafson: *Scand. J. Metall.*, 1985, vol. 14, pp. 259–67.
19. R.W. Heckel and H.W. Paxton: *Trans. ASM*, 1961, vol. 53, p. 539.
20. V.F. Zackay and H.I. Aaronson: *Decomposition of Austenite by Diffusional Processes*, Interscience Publishers, New York, 1962.
21. J.W. Cahn, W.B. Hillig, and G.W. Sears: *Acta Metall.*, 1964, vol. 12, pp. 1421–39.
22. G.J. Jones and R.K. Trivedi: *J. Appl. Phys.*, 1971, vol. 42, pp. 4299–4304.
23. G. Spanos, R.A. Masumura, R.A. Vandermeer, and M. Enomoto: *Acta Metall. Mater.*, 1994, vol. 42, pp. 4165–76.
24. J.J. Hoyt: *Acta Mater.*, 2013, vol. 61, pp. 4953–60.
25. W. Piyawit, W.Z. Xu, S.N. Mathaudhu, J. Freudenberger, J.M. Rigsbee, and Y.T. Zhu: *Mater. Sci. Eng. A*, 2014, vol. 610, pp. 85–90.
26. S.J. Clark, Y. Lan, A. Rahnama, V. Janik, and S. Sridhar: *ISIJ Int.*, 2019, vol. 59, pp. 573–82.
27. M.Y. Chen, M. Gouné, M. Militzer, Y. Bréchet, and J.R. Yang: *Metall. Mater. Trans. A Phys. Metall. Mater. Sci.*, 2014, vol. 45, pp. 5351–61.
28. G.J. Shiflet, M.A. Mangan, and W.G. Meng: *Interface Sci.*, 1998, vol. 6, pp. 133–54.
29. R.W. Heckel, J.H. Smith, and H.W. Paxton: *Trans. Metall. Soc. AIME*, 1960, vol. 218, pp. 566–68.
30. C. Atkinson: *Proc. R. Soc. Lond. A.*, 1981, vol. 378, pp. 351–68.
31. C. Atkinson: *Proc. R. Soc. Lond. A.*, 1982, vol. 384, pp. 107–33.
32. M.V. Kral and G. Spanos: *Acta Mater.*, 2003, vol. 51, pp. 301–11.
33. E. Kozeschnik: *Modeling Solid-State Precipitation*, Momentum Press, New York, 2012.
34. L. Onsager: *Phys. Rev.*, 1931, vol. 37, pp. 405–26.
35. L. Onsager: *Phys. Rev.*, 1931, vol. 38, pp. 2265–79.
36. J. Svoboda, I. Turek, and F.D. Fischer: *Philos. Mag.*, 2005, vol. 85, pp. 3699–3707.
37. J.O. Andersson, T. Helander, L. Höglund, P. Shi, and B. Sundman: *Calphad*, 2002, vol. 26, pp. 273–312.
38. B. Miesenberger, E. Kozeschnik, B. Milkereit, P. Warczok, and E. Povoden-Karadeniz: *Materialia*, 2022, vol. 25, 101538.
39. B. Sonderegger and E. Kozeschnik: *Metall. Mater. Trans. A*, 2009, vol. 40A, pp. 499–510.
40. B. Sonderegger and E. Kozeschnik: *Scr. Mater.*, 2009, vol. 60, pp. 635–38.
41. R.L. Fullman: *JOM*, 1953, vol. 5, pp. 447–52.
42. G. Spanos and H.I. Aaronson: *Acta Metall. Mater.*, 1990, vol. 38, pp. 2721–32.
43. R.A. Vandermeer: *Acta Metall. Mater.*, 1990, vol. 38, pp. 2461–70.